Band-Passing Nonlinearity in Reset Elements

Nima Karbasizadeh, *Member, IEEE*, Ali Ahmadi Dastjerdi, *Member, IEEE*, Niranjan Saikumar, *Member, IEEE*, and S. Hassan HosseinNia, *Senior Member, IEEE*

***Abstract*— This article addresses nonlinearity in reset elements and its effects. Reset elements are known for having less phase lag based on describing function (DF) analysis compared to their linear counterparts; however, they are nonlinear elements and produce higher-order harmonics. This article investigates the steady-state higher-order harmonics for reset elements with one resetting state and proposes an architecture and a method of design that allows for band-passing the nonlinearity and its effects, namely, higher-order harmonics and phase advantage. The nonlinearity of reset elements is not entirely useful for all frequencies, for example, they are useful for reducing phase lag at crossover frequency regions; however, higher-order harmonics can compromise tracking and disturbance rejection performance at lower frequencies. Using the proposed "phase shaping" method, one can selectively suppress the nonlinearity of a single-state reset element in a desired range of frequencies and allow the nonlinearity to provide its phase benefit in a different desired range of frequencies. This can be especially useful for the reset elements in the framework of the "constant in gain, lead in phase" (CgLp) filter, which is a newly introduced nonlinear filter, bound to circumvent the well-known linear control limitation—the waterbed effect.**

***Index Terms*— Higher-order harmonics, mechatronics, motion control, nonlinear control, precision motion control, reset control, shaping nonlinearity.**

I. Introduction

THE growing demand on precision, bandwidth, and robustness of controllers in fields like precision motion control are pushing linear control to its limits [1]. Fundamental limits of linear controllers, namely, Bode's phase gain relationship or Bode's sensitivity integral theorem, a.k.a., "the waterbed effect" [2], have made researchers and industries change course toward nonlinear control to circumvent these limitations [3]. Reset control is one such nonlinear technique that has gained significant prominence in recent times [4], [5], especially in the precision motion control field.

The reset control technique was first introduced by Clegg [6] as a nonlinear integrator and its advantage was described in [7] in terms of reducing phase lag compared to its linear counterparts. The main idea of reset control is to reset a subset of controller states when a predefined resetting condition is met. More sophisticated reset elements were developed over the years, namely, first-order reset element (FORE) [8], generalized first-order reset element (GFORE) [9] and second-order reset element (SORE) [10]. These reset elements were used in different capacities such as phase lag reduction, decreasing sensitivity peak, narrowband and broadband phase compensation, a guarantee of exponential convergence, and approximating the complex-order behavior [11]–[19]. Furthermore, they have been used for different applications, especially precision motion control [20]. A new reset-based architecture was recently proposed by [21], which has a constant gain while providing phase lead in a broad range of frequencies. This architecture, named "constant in gain, lead in phase" (CgLp), can completely replace or take up a significant portion of derivative duties in the framework of PID. The stability of reset elements is studied in the literature from different aspects [22], [23].

Being a nonlinear controller, reset elements produce higher-order harmonics, which in turn makes reset control two-edged. While it is capable of overcoming linear control limitations, the existence of higher-order harmonics can compromise the performance of the system [24]. Recently, researchers found describing function (DF) method for analyzing the reset elements in the frequency domain [9] insufficient, since it neglects the effect of higher-order harmonics. A generalized form of the DF method which accounts for higher-order harmonics called higher-order sinusoidal input describing function (HOSIDF) [25] was adopted for reset elements in [26] and [27]. There are efforts in the literature to reduce the adverse effects of higher-order harmonics in one frequency or by tuning reset element parameters or finding the optimal sequence of elements [24], [28]–[32]. However, to the best of the authors' knowledge, there is no systematic approach in the literature for deliberately reducing higher-order harmonics to a desired upper bound in a range of frequencies.

The main benefit of reset elements is the reduction of phase lag with respect to their linear counterparts. This characterization is beneficial in the crossover frequency region and has no clear benefit at other frequencies. Furthermore, higher-order harmonics compromise the performance of the system in terms of tracking precision and disturbance rejection which is basically discussed in the loop-shaping method at lower frequencies [30], [33]. Thus, providing a method to bandpass the nonlinearity and in turn higher-order harmonics seems

Manuscript received 8 June 2021; revised 5 October 2021 and 20 January 2022; accepted 14 May 2022. Date of publication 9 June 2022; date of current version 28 December 2022. This work was supported by the Nederlandse Organisatie voor Wetenschappelijk Onderzoek (NWO), through the Open Technology Program (OTP) Applied and Engineering Sciences (AES) Project, under Grant #16335. Recommended by Associate Editor J. T. Gravdahl. *(Corresponding author: S. Hassan HosseinNia.)*

The authors are with the Department of Precision and Microsystem Engineering, Delft University of Technology, 2628CD Delft, The Netherlands (e-mail: n.karbasizadehesfahani@tudelft.nl; a.ahmadidastjerdi@tudelft.nl; n.saikumar@tudelft.nl; s.h.hosseinniakani@tudelft.nl).

Color versions of one or more figures in this article are available at https://doi.org/10.1109/TCST.2022.3178043.

Digital Object Identifier 10.1109/TCST.2022.3178043

This work is licensed under a Creative Commons Attribution 4.0 License. For more information, see https://creativecommons.org/licenses/by/4.0/

logical to help keep the positive edge of reset elements while limiting its negative edge.

The main contribution of this article is the investigation of higher-order harmonics in reset elements with one resetting state and proposing an architecture and a method of design called "phase shaping" to allow for band-passing nonlinearity in reset elements. In other words, using the proposed architecture and phase shaping method one can create a reset element, for example, a Clegg integrator, a FORE, or a CgLp, which is nonlinear in a range of frequencies while it acts linearly in terms of steady-state response at other frequencies. Meaning that the element will limit its phase benefits to where it is needed and will have reduced higher-order harmonics at other frequencies. The article also investigates the performance of the proposed element in the framework of CgLp and shows that using the proposed method the performance of the CgLp element will be significantly improved.

The remainder of this article is organized as follows. Section II presents the preliminaries. Section III introduces and discusses the architecture of the proposed reset element and investigates its HOSIDF. Section IV will propose the design and tuning method called phase-shaping. The following one will introduce an illustrative example and verify the discussions in practice. Finally, the article concludes with some remarks and recommendations about ongoing works.

II. Preliminaries

This section discusses the preliminaries of this study.

A. General Reset Controller

Following is a general form of a reset controller [34]:

$$\sum_R := \begin{cases} \dot{x}_r(t) = A_r x_r(t) + B_r e(t), & \text{if } e(t) \neq 0 \\ x_r(t^+) = A_\rho x_r(t), & \text{if } e(t) = 0 \\ u(t) = C_r x_r(t) + D_r e(t) \end{cases} \tag{1}$$

where $\sum_R$ is the reset controller and A_r, B_r, C_r, D_r are the state space matrices of the base linear system and $A_\rho = \text{diag}(\gamma_1, \ldots, \gamma_n)$ is called reset matrix. This matrix contains the reset coefficients for each state which are denoted by $\gamma_1, \ldots, \gamma_n$. $x_r(t^+)$ represents the value of the reset state exactly after reset action. The controller's input and output are represented by $e(t)$ and $u(t)$, respectively.

B. H_β Condition

The quadratic stability of the closed-loop reset system when the base linear system is stable can be examined by the following condition [5], [35]:

Theorem 1: There exists a constant $\beta \in \Re^{n_r \times 1}$ and positive definite matrix $P_\rho \in \Re^{n_r \times n_r}$, such that the restricted Lyapunov equation

$$P > 0, \; A_{\text{cl}}^T P + P A_{\text{cl}} < 0 \tag{2}$$

$$B_0^T P = C_0 \tag{3}$$

has a solution for P, where C_0 and B_0 are defined by

$$C_0 = \begin{bmatrix} \beta C_p & 0_{n_r \times n_{nr}} & P_\rho \end{bmatrix}, \quad B_0 = \begin{bmatrix} 0_{n_p \times n_r} \\ 0_{n_{nr} \times n_r} \\ I_{n_r} \end{bmatrix}. \tag{4}$$

and

$$A_\rho^T P_\rho A_\rho - P_\rho \leq 0 \tag{5}$$

where A_{cl} is the closed-loop A-matrix. n_r is the number of states being reset and n_{nr} being the number of nonresetting states and n_p is the number states for the plant. A_p, B_p, C_p, D_p are the state space matrices of the plant.

C. Describing Functions

Because of its nonlinearity, the steady-state response of a reset element to a sinusoidal input is not sinusoidal. Thus, its frequency response should be analyzed through approximations like DF method [9]. However, the DF method only takes the first harmonic of Fourier series decomposition of the output into account and neglects the effects of the higher-order harmonics. As shown in [24], this simplification can sometimes be significantly inaccurate. To have more accurate information about the frequency response of nonlinear systems, a method called "higher-order sinusoidal input describing function" (HOSIDF) has been introduced in [25]. This method was developed in [26] and [27] for reset elements defined by (1) as follows:

$$\begin{aligned} G_n(\omega) &= \begin{cases} C_r(j\omega I - A_r)^{-1}(I + j\Theta(\omega))B_r + D_r, \\ \quad n = 1 \\ C_r(j\omega n I - A_r)^{-1} j\Theta(\omega) B_r, \\ \quad \text{odd } n > 2 \\ 0, \quad \text{even } n \geq 2 \end{cases} \\ \Theta(\omega) &= -\frac{2\omega^2}{\pi}\Delta(\omega)[\Gamma(\omega) - \Lambda^{-1}(\omega)] \\ \Lambda(\omega) &= \omega^2 I + {A_r}^2 \\ \Delta(\omega) &= I + e^{\frac{\pi}{\omega}A_r} \\ \Delta_\rho(\omega) &= I + A_\rho e^{\frac{\pi}{\omega}A_r} \\ \Gamma(\omega) &= \Delta_\rho^{-1}(\omega) A_\rho \Delta(\omega) \Lambda^{-1}(\omega) \end{aligned} \tag{6}$$

where $G_n(\omega)$ is the nth harmonic describing function for sinusoidal input with frequency of ω.

According to definition of reset elements in open-loop in (1), assuming $e(t) = \sin(\omega t)$, the resetting condition will be $\sin(\omega t) = 0$ and the reset instants will be $t_k = (k\pi/\omega)$. However, if by changing the architecture of reset element, one can manage to change the resetting condition to the following:

$$\sum_R := \begin{cases} \dot{x}_r(t) = A_r x_r(t) + B_r e(t), & \text{if } \sin(\omega t - \varphi) \neq 0 \\ x_r(t^+) = A_\rho x_r(t), & \text{if } \sin(\omega t - \varphi) = 0 \\ u(t) = C_r x_r(t) + D_r e(t) \end{cases} \tag{7}$$

means that the signal which determines the reset instants is phase shifted by φ. In other words, if one changes the reset instants, $t_k = (k\pi + \varphi/\omega)$, while maintaining the input, $e(t)$, then HOSIDF will change to [27]

$$G_{\varphi n}(\omega) = \begin{cases} C_r(A_r - j\omega I)^{-1}\Theta_\varphi(\omega) \\ \qquad + C_r(j\omega I - A_r)^{-1} B_r + D_r, \quad n = 1 \\ C_r(A_r - j\omega n I)^{-1}\Theta_\varphi(\omega), \quad \text{odd } n > 2 \\ 0, \quad \text{even } n \geq 2 \end{cases}$$

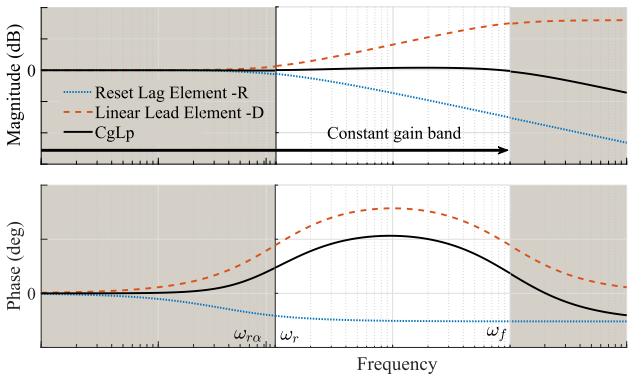

Fig. 1. Concept of using a combination of a reset lag and a linear lead element to form a CgLp element. The figure is from [21].

$$\Theta_\varphi(\omega) = \frac{-2j\omega e^{-j\varphi}}{\pi}\Omega(\omega)(\omega I\cos(\varphi) + A_r\sin(\varphi))\Lambda^{-1}(\omega)B$$
$$\Omega(\omega) = \Delta(\omega) - \Delta(\omega)\Delta_\rho^{-1}(\omega)A_\rho\Delta(\omega). \tag{8}$$

It will be discussed later in the article that (8) can be used to obtain the HOSIDF of the proposed architecture, where the phase shift, φ, is implemented in a set of frequencies.

D. Constant in Gain, Lead in Phase (CgLp)

According to [21], CgLp is a broadband phase compensation element whose first harmonic gain behavior is constant while providing a phase lead. Originally, two architectures for CgLp are suggested using FORE or SORE, both consisting in a reset lag element in series with a linear lead filter, namely $\sum_R$ and D. For FORE CgLp

$$\sum_R = \frac{1}{s/\omega_{r\alpha}+1}\xrightarrow{A_\rho}, \quad D(s) = \frac{s/\omega_r + 1}{s/\omega_f + 1}. \tag{9}$$

The arrow indicates that the states of element are reset according to A_ρ; that is, are multiplied by A_ρ when the reset condition is met; see (1). For SORE CgLp,

$$\sum_R = \frac{1}{(s/\omega_{r\alpha})^2 + (2s\beta/\omega_{r\alpha}) + 1}\xrightarrow{A_\rho}$$
$$D(s) = \frac{(s/\omega_r)^2 + (2s\beta/\omega_r) + 1}{(s/\omega_f)^2 + (2s/\omega_f) + 1}. \tag{10}$$

In (9) and (10), $\omega_{r\alpha} = \omega_r/\alpha$, α is a tuning parameter accounting for a shift in the corner frequency of the filter due to resetting action, β is the damping coefficient, and $[\omega_r, \omega_f]$ is the frequency range where the CgLp will provide the required phase lead.

The main idea behind the CgLp is to take the phase advantage of the reset lag element over its linear counterpart and use it in combination with a corresponding lead element to create a broadband phase lead. Ideally, the gain of the reset lag element should be canceled out by the gain of the corresponding linear lead element, which creates a constant gain behavior. The concept is depicted in Fig. 1.

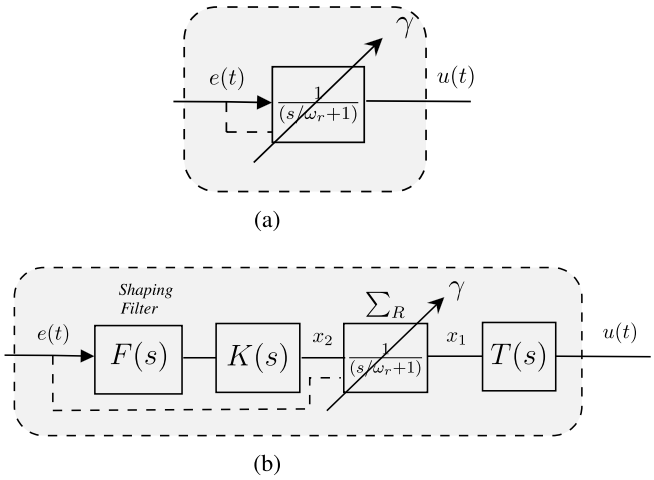

Fig. 2. Block diagrams of a conventional FORE and a single-state reset element including a shaping filter proposed by this article. (a) Conventional FORE. (b) Single-state reset element including a shaping filter.

III. Single-State Reset Element Including a Shaping Filter

This article proposes an architecture for reset elements with only one resetting state including a shaping filter. This section will analyze the HOSIDF of such an element and its specific properties. The block diagram of the proposed element is presented in Fig. 2(b).

HOSIDF of this element can be found using (6) with

$$A_\rho = \text{diag}(\underbrace{1,\ldots,1}_{n_F+n_K}, \gamma, \underbrace{1,\ldots,1}_{n_T})$$

where n_F, n_K, and n_T are the number of states for linear filters $F(s)$, $K(s)$, and $T(s)$, respectively.

However, in this article, (8) will be used, since it will reveal more useful information. Let us define

$$\psi(\omega) := \angle\frac{X_1(j\omega)}{E(j\omega)} \quad \text{for } \gamma = 1. \tag{11}$$

It is to be noted that ψ is defined in a linear context and is based on base linear system and $X_1(j\omega)$ and $E(j\omega)$ are the Fourier transform of the signals $x_1(t)$ and $e(t)$, respectively, in Fig. 2(b).

Theorem 2: The higher-order harmonics of the architecture in Fig. 2(b) is an exponential function of $\psi(\omega)$

$$H_n(\omega) = f(n,\omega)(1 - e^{-j2\psi}) \tag{12}$$

where

$$f(n,\omega) = C_r(A_r - j\omega nI)^{-1}\frac{\omega e^{-j\tan^{-1}\left(\frac{\omega}{\omega_r}\right)}}{\pi\sqrt{1+\left(\frac{\omega}{\omega_r}\right)^2}}$$
$$\times\left((1-\gamma)\left(1+\gamma e^{\frac{-\pi\omega_r}{\omega}}\right)^{-1}\left(1+e^{\frac{-\pi\omega_r}{\omega}}\right)\right). \tag{13}$$

Proof: Let us temporarily denote $Q(s) := F(s)K(s)$. For HOSIDF analysis, $e(t) = \sin(\omega t)$, thus

$$x_2(t) = |Q(j\omega)|\sin(\omega t + \phi(\omega)) \tag{14}$$

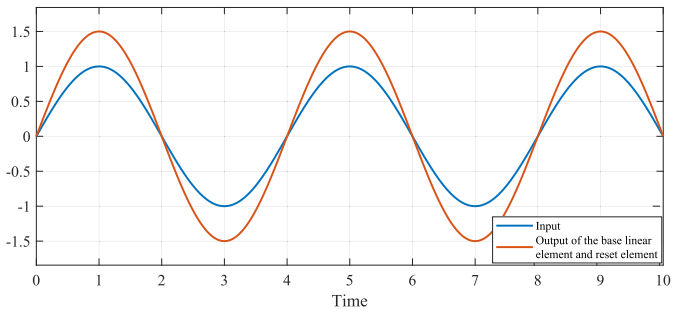

Fig. 3. Assuming that the output of the base linear element ($x_1(t)$ for $\gamma = 1$) for a reset element has no phase shift with respect to its input ($e(t)$), the output of the reset element itself ($x_1(t)$ for $\gamma \neq 1$) will match the base linear element output at steady state.

where $\phi(\omega) = \angle Q(j\omega)$. From the block diagram of Fig. 2(b), we have

$$\phi(\omega) = \psi(\omega) + \tan^{-1}\left(\frac{\omega}{\omega_r}\right). \tag{15}$$

It can be readily seen that input to the $\sum_R$ is $x_2(t)$ while the resetting condition is determined by $e(t)$, which have a phase difference. One can find the nth harmonic, $H_n(\omega)$, by the following equation:

$$H_n(\omega) = Q(j\omega)G_{\varphi n}(\omega)T(jn\omega) \tag{16}$$

where $G_{\varphi n}$ can be obtained using (8) using

$$\varphi = \phi(\omega) = \psi(\omega) + \tan^{-1}\left(\frac{\omega}{\omega_r}\right). \tag{17}$$

For $\sum_R$, in this article, we have

$$A_r = -\omega_r, \quad B_r = \omega_r, \quad C_r = 1, \quad D_r = 0, \quad A_\rho = \gamma. \tag{18}$$

Using (8), (17), and (18), after some simplifications we have

$$G_{\varphi n}(\omega) = \begin{cases} f(n,\omega)\left(1 - e^{-j2\psi}\right) \\ \quad + C_r(j\omega I - A_r)^{-1}B_r + D_r, & n = 1 \\ f(n,\omega)\left(1 - e^{-j2\psi}\right), & \text{odd } n > 2 \\ 0, \quad \text{even } n \geq 2. \end{cases} \tag{19}$$

□

Remark 1: Let us define

$$\omega_{lb} := \{\omega | \psi(\omega) = 0\}. \tag{20}$$

According to (8) and (19)

$$G_{\varphi n}(\omega_{lb}) = \begin{cases} C(j\omega_{lb}I - A_r)^{-1}B_r + D_r, & n = 1 \\ 0, & n \geq 2. \end{cases} \tag{21}$$

Remark 1 shows that for each frequency in ω_{lb}, all the higher-order harmonics will be zero; in other words, the element will act as its base linear system in terms of steady-state output. By way of explanation, when ψ is zero, the reset element, $\sum_R$, will reset its state to zero when the state value is already zero. Hence, the resetting action has no effect on the steady-state response. Fig. 3 depicts this situation. Obviously, in this situation, there exists no phase advantage for the reset element.

Remark 2: For a fixed value of ω, ω_r, and γ, the maximum of higher-order harmonics magnitude will happen when $\psi(\omega) = ((k+1)\pi/2), k \in \mathbb{Z}$.

Remark 3: For $\omega > 10\omega_r$, the phase of the first-harmonic of the reset element can be approximated by

$$\angle G_{\varphi 1}(\omega) \approx \tan^{-1}\left(\frac{U\sin(2\psi) - 1}{2U\sin^2(\psi)}\right) \tag{22}$$

where

$$U = \frac{2(1-\gamma)}{\pi(1+\gamma)}.$$

Thus, the phase of the first harmonic of the reset element for $\omega > 10\omega_r$ only depends on ψ and γ.

Remark 3 implies that at a frequency that is at least one decade higher than ω_r, different combinations of ψ and γ may result in the same first-harmonics phase for the reset element. Meanwhile, ψ and γ also affect the higher-harmonics magnitude as indicated in (19). Thus, in solving an optimization problem, one can find the best combination of ψ and γ for a desired first-harmonic phase and minimum higher-order harmonics magnitude.

IV. Phase Shaping Method

Theorem 2 and its following remarks constitute the main idea of the phase shaping method for band-passing nonlinearity in reset elements. Previous discussions revealed that the nonlinearity in the reset element and its two immediate consequences, namely, phase advantage and higher-order harmonics are dependent on $\psi(\omega)$. The proposed architecture in this article allows for shaping this phase difference, ψ, and consequently nonlinearity in a reset element.

From Fig. 2(b), we have

$$\psi(\omega) = \angle(F(j\omega)K(j\omega)R(j\omega)) \tag{23}$$

where $R(s)$ represents the base linear element for $\sum_R$. Let

$$K(s) = \frac{R^{-1}(s)}{s/\omega_f + 1} = \frac{s/\omega_r + 1}{s/\omega_f + 1} \tag{24}$$

which is the inverse of the $R(s)$ multiplied to a low-pass filter to make it proper. For a large enough ω_f,

$$\psi(\omega) = \angle F(j\omega). \tag{25}$$

Shaping $\psi(\omega)$ is now reduced to shaping the phase of $F(s)$. If one designs $F(s)$ to have a phase plot as depicted in Fig. 4, the following will happen according to Theorem 2 and its following remarks.

1) Each zero-crossing frequency belongs to ω_{lb}, where the reset element produces no higher-order harmonics the steady state. These frequencies will be seen as higher-order harmonic notches in HOSIDF.
2) For frequencies out of $[\omega_l, \omega_h]$, one can upper bound nonlinearity by determining ψ_b. For a small enough ψ_b, higher-order harmonics can be approximated to zero. There will be no phase advantage for reset elements at these frequencies.

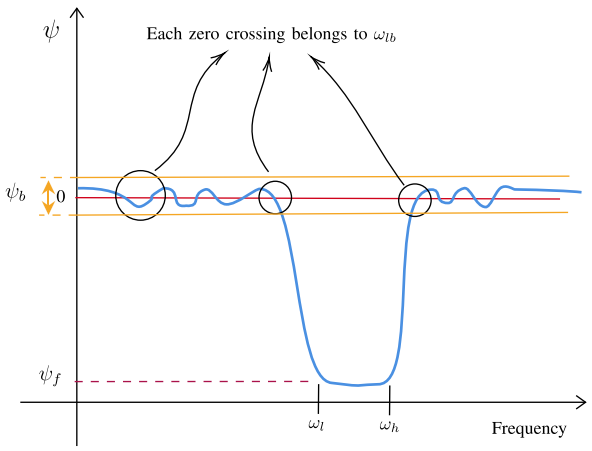

Fig. 4. Desired shape of phase for $\psi(\omega)$ for band-passing nonlinearity.

3) For frequencies in $[\omega_l, \omega_h]$, the reset element will produce high-order harmonics and will have a phase advantage.
4) ψ_f and γ determine the phase advantage of the reset element in $[\omega_l, \omega_h]$.

It can be concluded that by this design, the nonlinearity of the reset element is band-passed in $[\omega_l, \omega_h]$. The details on how to design $F(s)$ to have this phase behavior will be discussed in the next section.

A. Band-Passed CgLp

In order to create a band-passed CgLp, let

$$T(s) = F^{-1}(s) \tag{26}$$

then we have

$$H_n(\omega) = \begin{cases} K(j\omega)G_{\varphi n}(\omega), & n = 1 \\ F(j\omega)K(j\omega)G_{\varphi n}(\omega)F^{-1}(jn\omega), & n > 1 \end{cases}$$
$$\varphi(\omega) = \angle F(j\omega) + \tan^{-1}\left(\frac{\omega}{\omega_r}\right) \tag{27}$$

where $F(s)$ and $K(s)$ should be designed based on the guidelines of the phase shaping method. As mentioned above, it has to be noted that resetting action will cause a shift in the corner frequency of $R(s)$ [21]. In order to account for this frequency shift, an additional filter of

$$W(s) = \frac{(s/\omega_{r\alpha} + 1)}{(s/\omega_r + 1)} \tag{28}$$

can be used in $T(s)$

$$T(s) = F^{-1}(s)W(s). \tag{29}$$

In order to verify the discussion, a CgLp element has been band-passed in $(1, 10)$ rad/s. The HOSIDF analysis of the band-passed CgLp is compared with a conventional one in Fig. 5. Both CgLps have $\omega_r = 0.5$ rad/s, γ is chosen to get approximately same phase advantage. As expected, the shaped ψ has made higher-order harmonics zero at frequencies in ω_{lb} and almost zero at other frequencies out of $[1, 10]$ rad/s. The phase advantage is also limited to the band specified.

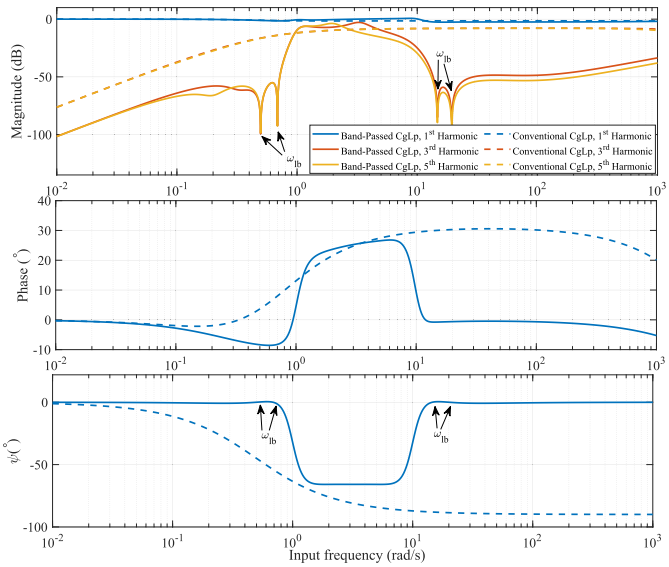

Fig. 5. Comparison of HOSIDF of a band-passed CgLp with a conventional one, along with their ψ plot. $\omega_r = 0.5$ rad/s and γ is 0.2 and 0.35 for band-passed CgLp and conventional one, respectively.

It is noteworthy that by changing the ψ shape in (ω_l, ω_h), one can change the shape of phase advantage. This can be useful in creating properties like iso-damping behavior [36]–[38].

B. Band-Passed Clegg Integrator and Band-Passed FORE

Following the same design approach and by letting

$$T(s) = \frac{F^{-1}(s)}{s} \tag{30}$$

one can create a band-passed Clegg integrator. Likewise, a band-passed FORE can be created by

$$T(s) = \frac{F^{-1}(s)}{s/\omega_{rr} + 1} \tag{31}$$

where ω_{rr} will be the new corner frequency for the FORE. Figs. 6 and 7 compares the HOSIDF of a band-passed Clegg integrator and a band-passed FORE with their conventional counterparts. Both reset elements are band-passed in $[1, 10]$ rad/s. As mentioned above, reset elements are usually known and used for their phase lag reduction compared to their linear counterparts [8], [39], [40]. Phase lag reduction is mainly useful in the crossover frequency region, and in other regions, it does not have a clear benefit. Thus, due to the ill effect of higher-order harmonics especially for tracking and disturbance rejection, the proposed method is useful to bandpass the nonlinearity of these reset elements and its consequent benefits and ill effects on the crossover frequency region.

V. Designing the Shaping Filter

This section proposes a method to design the shaping filter, $F(s)$, such that its phase mimics the schematic shape of Fig. 4. The first parameter to consider is ψ_f, which affects the phase of the reset element. Assuming the nonlinearity of the reset element is being band-passed in the crossover frequency region, if ω_r is less than $\omega_c/10$, where ω_c is the

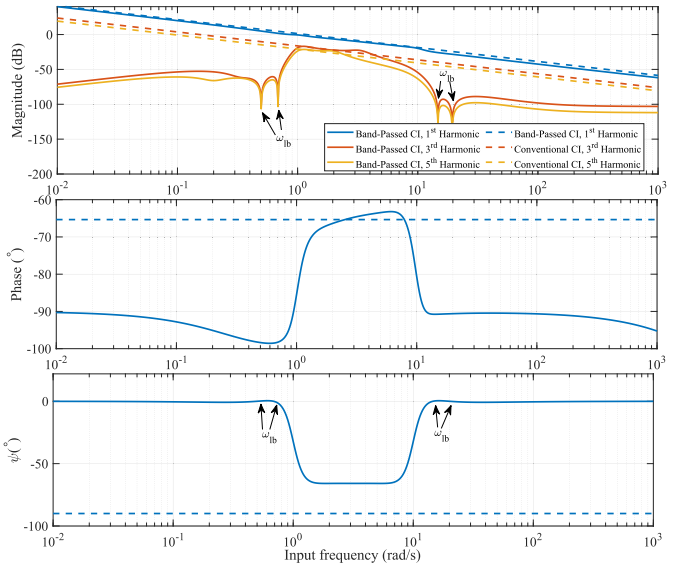

Fig. 6. Comparison of HOSIDF of a band-passed Clegg integrator with a conventional one, along with their ψ plot. γ is 0.2 and 0.47 for band-passed Clegg Integrator and conventional one, respectively. For band-passed Clegg, $\omega_r = 0.5$ rad/s.

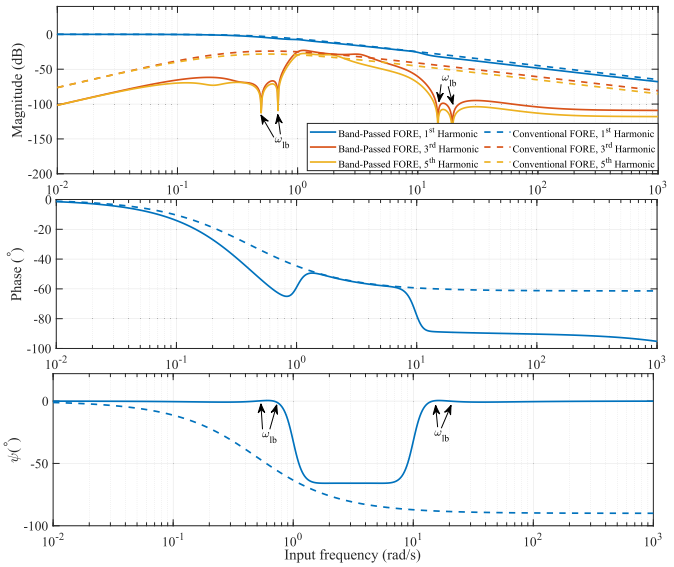

Fig. 7. Comparison of HOSIDF of a band-passed FORE with a conventional one, along with their ψ plot. $\omega_r = 0.5$ rad/s and γ is 0.2 and 0.4 for band-passed FORE and conventional one, respectively. For band-passed FORE, $\omega_{rr} = 0.5$ rad/s.

crossover frequency, one can choose a combination of γ and ψ_f according to (22) to achieve the desired first-harmonic phase of the reset element at ω_c.

The suggested architecture for the shaping filter consists of a lag filter, a notch, and an anti-notch filter. The notch and the anti-notch filters should be placed at ω_h and ω_l, respectively. Since it is required for the phase of the shaping filter to reach a certain value in the passing band, this method requires a flat phase behavior which is not an integer multiple of 90°. This is achievable using fractional lag filters; thus, the poles and zeros of the lag filter can be placed according to guidelines of the CRONE approximation of a fractional-order element [41]. Such a placement will simplify the calculations.

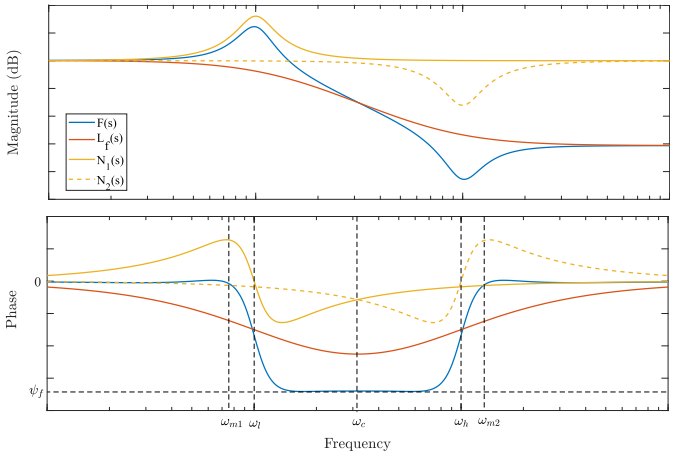

Fig. 8. Bode diagram of the composition of $F(s)$.

The CRONE approximation is

$$\left(\frac{s/\omega_l + 1}{s/\omega_h + 1}\right)^{\lambda} \approx C \prod_{m=1}^{N} \frac{1 + \frac{s}{\omega_{z,m}}}{1 + \frac{s}{\omega_{p,m}}} \tag{32}$$

$$\omega_{z,m} = \omega_l \left(\frac{\omega_h}{\omega_l}\right)^{\frac{2m-1-\lambda}{2N}} \tag{33}$$

$$\omega_{p,m} = \omega_l \left(\frac{\omega_h}{\omega_l}\right)^{\frac{2m-1+\lambda}{2N}} \tag{34}$$

where $\lambda \in \Re^-$ and N is number of poles and zeros. CRONE makes sure that the poles and zeros are placed in equal distance in the logarithmic scale. C is the tuning parameter for adjusting the gain of the approximation. However, in this article, only the phase behavior of this filter is of interest since the first-order gain behavior of this element will be canceled out according to (27). Thus, for the sake of simplicity, one can use $C = 1$.

The proposed design of the shaping filter is

$$F(s) = N_1(s) L_f(s) N_2(s) \tag{35}$$

$$L_f(s) = \left(\frac{s/\omega_l + 1}{s/\omega_h + 1}\right)^{\lambda} \tag{36}$$

$$N_1(s) = \frac{(s/\omega_l)^2 + s/\omega_l + 1}{(s/\omega_l)^2 + s/(q\omega_l) + 1} \tag{37}$$

$$N_2(s) = \frac{(s/\omega_h)^2 + s/(q\omega_h) + 1}{(s/\omega_h)^2 + s/\omega_h + 1}. \tag{38}$$

Thus, there are two parameters to tune, namely, λ and q. According to Fig. 8 and criteria mentioned in Section IV for the shaping filter, two constraints can be introduced to find the proper value for λ and q

$$\angle F(j\omega_c) = \psi_f \tag{39}$$

$$\angle F(j\omega_{m1}) = \angle F(j\omega_{m2}) = \varepsilon_1 \tag{40}$$

where ε_1 is a small positive value and

$$\omega_{m1} \in (0, \omega_l) \mid \frac{d}{d\omega} \angle N_1(j\omega_{m1}) = 0 \tag{41}$$

$$\omega_{m2} \in (\omega_h, +\infty) \mid \frac{d}{d\omega} \angle N_2(j\omega_{m2}) = 0. \tag{42}$$

Equation (40) ensures that the phase of the shaping filter remains close to zero and crosses the zero line two times before ω_l and two times after ω_h. By symmetry, constraints will be simplified to

$$\angle L_f(j\omega_c) + 2\angle N_1(j\omega_c) = \psi_f \tag{43}$$
$$\angle L_f(j\omega_{m1}) + \angle N_1(j\omega_{m1}) = \varepsilon_2. \tag{44}$$

As a rule of thumb, one can choose $\varepsilon_2 = \pi/180$ rad.

In this article, without loss of generality, it is assumed that the band-passing range is one decade, that is, $\omega_h = 10\omega_l$ and the equations are derived in the following.

Assuming $\omega_h = 10\omega_l$, we have $\omega_c = \sqrt{10}\omega_l$, thus

$$\angle L_f(j\omega_c) \approx \lambda\left(\tan^{-1}\left(\sqrt{10}\right) - \tan^{-1}\left(\frac{1}{\sqrt{10}}\right)\right) \tag{45}$$
$$\angle N_1(j\omega_c) = \tan^{-1}\left(\frac{\sqrt{10}}{9q}\right) - \tan^{-1}\left(\frac{\sqrt{10}}{9}\right) \tag{46}$$
$$\angle L_f(j\omega_{m1}) = \lambda\left(\tan^{-1}(\zeta) - \tan^{-1}(\zeta/10)\right) \tag{47}$$
$$\angle N_1(j\omega_{m1}) = \tan^{-1}\left(\frac{\zeta}{1-\zeta^2}\right) - \tan^{-1}\left(\frac{\zeta/q}{1-\zeta^2}\right) \tag{48}$$

where

$$\zeta = \frac{\omega_{m1}}{\omega_l} = \frac{\sqrt{2}}{2}\sqrt{\frac{2q+1-\sqrt{1+4q}}{q}}. \tag{49}$$

VI. Illustrative Example

In order to illustrate the application of the proposed architecture and method in precision motion control, three controllers have been designed and their performance has been compared. The three controllers are a band-passed CgLp, a conventional CgLp designed based on guidelines of [21] and a PID.

A. Plant

The plant which is used for practical implementation is a custom-designed precision stage that is actuated with the use of a Lorentz actuator. This stage is linear-guided using two flexures to attach the Lorentz actuator to the base of the stage and actuated at the center of the flexures. With a laser encoder, the position of the precision stage is read out with a 10-nm resolution. A picture of the setup can be found in Fig. 9. The identified transfer function for the plant is

$$G(s) = \frac{3.038\text{e}4}{s^2 + 0.7413s + 243.3}. \tag{50}$$

Generally precision motion setups can be modeled as mass-spring-damper systems as this is the case for this setup. Fig. 10 shows the measured frequency response and that of the identified model.

B. Controller Design Approach

Controllers are designed for a bandwidth of $\omega_c = 100$ Hz and a phase margin of 40°. The block diagram of the closed-loop system for CgLps is presented in Fig. 11. The tamed differentiator [33] is designed such that the linear part of the controller provides 10° of PM for the system and CgLps are designed to provide the remaining 30°. The main

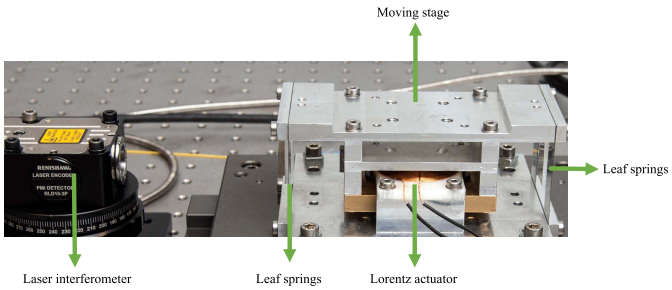

Fig. 9. Custom-designed precision stage used for comparison of controllers performance.

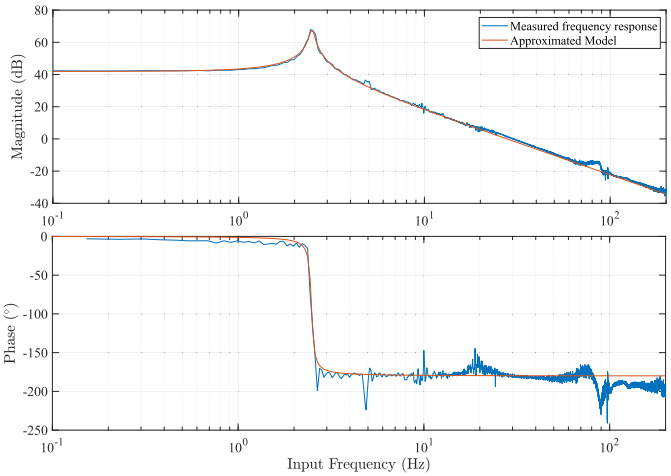

Fig. 10. Measured frequency response of the plant and corresponding identified model.

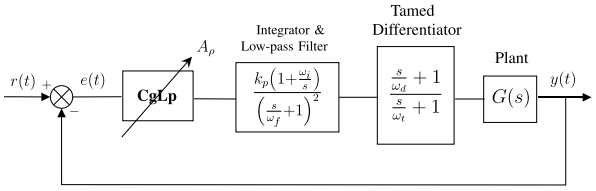

Fig. 11. Designed control architecture to compare the performance of the controllers.

reason for the existence of the tamed differentiator for CgLp controllers is stabilizing the base linear system, which is one of the necessary conditions for stability using the H_β theorem. For the case of the PID controller, the whole required PM is provided through a tamed differentiator.

Table I shows the parameters for the designed controllers. Fig. 12 shows the open-loop HOSIDF analysis for them including the plant. As expected, CgLp controllers show a higher first-order harmonic gain than PID in lower frequencies, while they have the same phase margin as PID. However, due to the design method presented in this article, the band-passed CgLp shows a significant decrease in higher-order harmonics than the conventional one. Consequently, one can expect an improvement in precision in the results of band-passed CgLp.

The reset controllers has been checked regarding the H_β condition as presented in Theorem 1. Both reset controllers

TABLE I

PARAMETERS OF THE DESIGNED CONTROLLERS. FREQUENCIES ARE IN HZ

Controller	ω_i	ω_d	ω_t	ω_f	ω_r	γ	ψ	λ	q
Band-passed CgLp	10	60.6	165	1000	5	-0.05	$-57.34°$	-0.69	2.21
FORE CgLp	10	60.6	165	1000	5	0.25	N/A	N/A	N/A
PID	10	27.0	370	1000	N/A	N/A	N/A	N/A	N/A

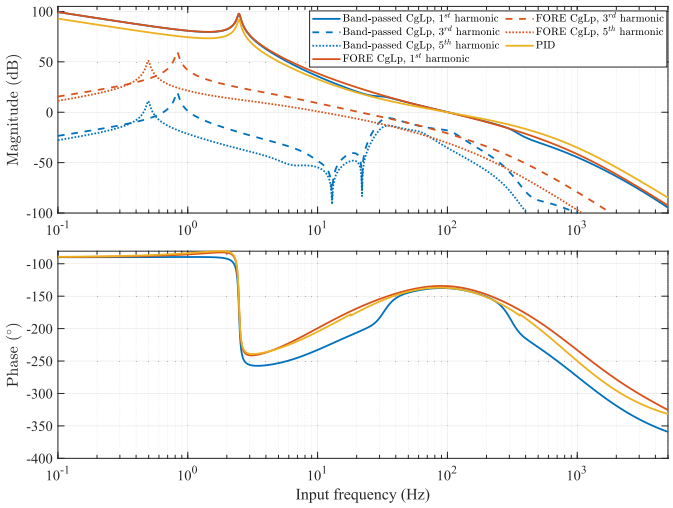

Fig. 12. Open-loop HOSIDF analysis of the designed controllers including the plant. At lower frequencies, first harmonic gain of band-passed CgLp and FORE CgLp are on top of each other.

satisfy the condition, thus, their quadratic closed-loop stability is guaranteed.

C. Practical Implementation

In order to validate the theories, architectures, and methods discussed, the designed controllers have been implemented in practice and their performance has been compared. The implementation was done using National Instruments CompactRIO with a sampling frequency of 10 kHz. The overall order of controller for PID, FORE CgLp, and Band-passed CgLp are 3, 5, and 16, respectively. Since high-end hardware for implementing the controller is used, the high order of Band-passed CgLp is feasible to implement, which is the case for most precision motion control system hardware.

Sinusoidal tracking of different frequencies and different amplitudes has been tested in practice for three designed controllers. Fig. 13 shows the error and control input of three controllers to track a 5-Hz sinusoidal input with an amplitude of 200 μm.

As it is shown in Fig. 13, band-passed CgLp has better steady-state precision than PID as it could be predicted by referring to Fig. 12. However, conventional CgLp due to the presence of higher-order harmonics cannot live up to the expectation of first-order DF. The Root Mean Square (RMS) of error for controllers are 0.346, 1.32, and 0.465 μm for the band-passed CgLp, the conventional one, and PID, respectively. The figures show a reduction of 25.7% and 74% in RMS of steady-state error for the band-passed CgLp with respect to PID and the conventional CgLp.

Fig. 13 also reveals another interesting characteristic of the band-passed CgLp. Reset controllers are known for having

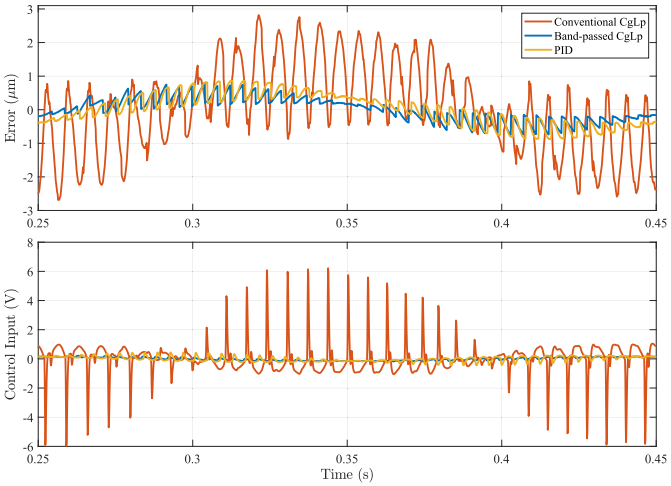

Fig. 13. Error and control input of designed controllers, measured in practice for a sinusoidal input of 5 Hz and amplitude of 0.2 mm.

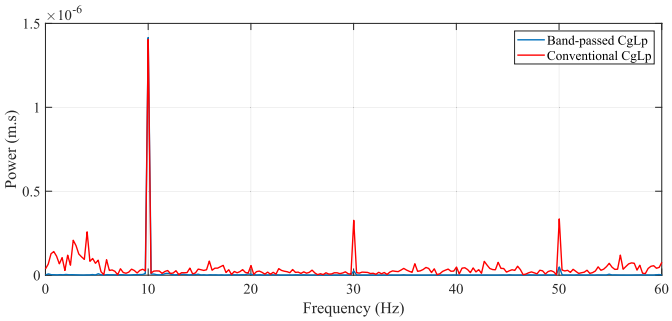

Fig. 14. Single-sided FFT spectrum of steady-state error for a sinusoidal input of 10 Hz. The amplitude of reference is 71.43 μm.

large peaks in control input which can saturate the actuator. However, the band-passed CgLp due to limited nonlinearity shows a much smaller control input with respect to the conventional CgLp. The maximum control input for controllers is 0.297, 6.980, and 0.448 V for the band-passed CgLp, the conventional one, and PID, respectively.

The main contribution of this article and designing band-passed CgLp is to limit nonlinearity to a range of frequencies and reduce it to other frequencies. Thus, it is expected that the band-passed CgLp has lower higher-order harmonics than the conventional ones in the range of [0.1–30] Hz. This was also verified in practical implementation as it is shown in the single-sided spectrum of Fast Fourier Transform (FFT) of steady-state error for a sinusoidal input of 10 Hz, presented in Fig. 14. From the figure, it can be observed that the third and the fifth harmonics, which are at 30 and 50 Hz, are significantly lower for band-passed CgLp. The same holds for other sinusoidal inputs with frequencies in [0.1, 30] Hz, however, they are not presented for the sake of brevity.

Furthermore, in order to have a broader view of tracking the performance of designed controllers, L_2 and L_∞ norm of their steady-state error for sinusoidal inputs of amplitude 71.43 μm and frequencies of 1–24 Hz in steps of 1 Hz is depicted in Fig. 15. The figure clearly shows a significant decrease of steady-state error for band-passed CgLp with respect to

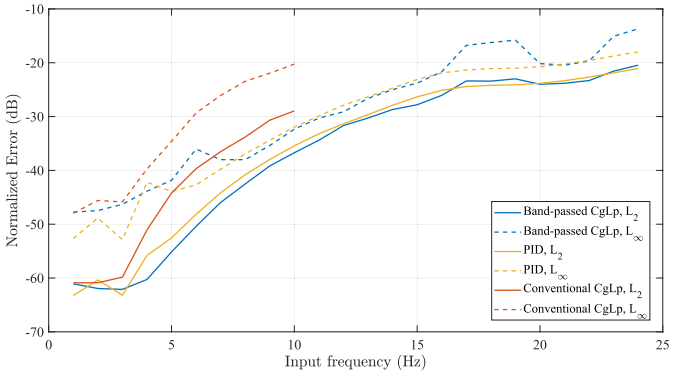

Fig. 15. L_2 and L_∞ norm of normalized steady-state error for sinusoidal inputs with amplitude of 71.43 μm and frequencies of 1–24 Hz with a step of 1 Hz. The error is normalized with respect to amplitude of input.

TABLE II

HARMONICS OF STEADY-STATE ERROR FOR SINUSOIDAL INPUTS OF 21, 22, AND 23 Hz. COLUMNS 2–5 SHOW HARMONICS IN m AND IN COLUMNS 5–8, HARMONICS ARE NORMALIZED BY THE AMPLITUDE OF INPUT AND PRESENTED IN dB

Freq. (Hz)	1st (m)	3rd (m)	5th (m)	7th (m)	1st (dB)	3rd (dB)	5th (dB)	7th (dB)
21	5.45e−6	4.54e−7	1.97e−7	7.23e−8	-22.33	-43.93	-51.15	-59.89
22	6.54e−6	1.92e−7	1.11e−7	3.80e−8	-20.75	-51.40	-56.10	-65.48
23	7.50e−6	1.64e−6	5.33e−7	1.22e−7	-19.56	-32.77	-42.52	-55.31

conventional one, indicating the adverse effect of higher-order harmonics in lower frequencies for tracking precision. Due to large peaks present in the control input of the conventional CgLp, tracking sinusoidal waves of frequencies larger than 10 Hz was not possible due to actuator saturation. Moreover, L_∞ norm (rms) of error for band-passed CgLp is lower than PID in almost the entire frequency range till 17 Hz. By resorting to Fig. 12, one can notice that from 17 Hz, the higher-order harmonics will increase for band-passed CgLp and decrease again at 22 Hz. The same trend holds for Fig. 15. At very low frequencies, that is, 1–3 Hz, higher-order harmonics of band-passed CgLp is relatively high, and thus the steady-state error. A possible suggestion to improve performance at these frequencies is designing a shaping filter such that a frequency within this range, for example, 2 Hz is included in ω_{lb}. This will reduce the higher-order harmonics in this range.

Remark 1 suggests that for every frequency in ω_{lb}, higher-order harmonics will be zero. However, in practice, due to practical challenges like discretization, quantization, and delay, it is expected that this claim does not hold completely. In other words, one can expect a decrease in higher-order harmonics to drop for frequencies in ω_{lb}. Table II presents the first, third, fifth, and seventh harmonics of steady-state error for sinusoidal inputs of 21, 22, and 23 Hz, where 22 Hz is in ω_{lb}. The harmonics are obtained using the FFT method. The significant drop in higher-order harmonics is observable for 22 Hz.

At last, in order to evaluate the performance of the proposed band-passed CgLp controller for multi-sinusoidal tracking, an input constituted of three sinusoidal wave was used. The reference which was used is

$$r(t) = 10^{-5}(1.5\sin(2\pi 13\ t) + 2.5\sin(2\pi 7\ t) + 5\sin(2\pi 5\ t)). \tag{51}$$

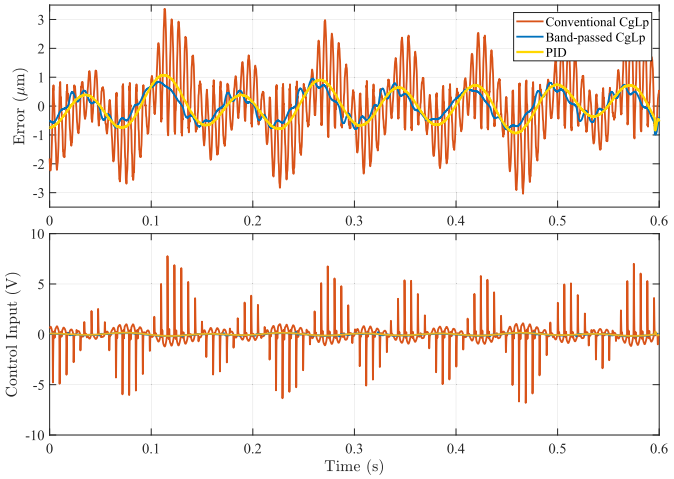

Fig. 16. Error and control input compared for three designed controllers for the input of (51). The rms of error is 0.463, 1.17, and 0.535 μm for band-passed CgLp, conventional CgLp, and PID, respectively. The maximum of steady-state error for controllers is 1.13, 3.47, and 1.18 μm.

Fig. 16 shows the error and control input for three designed controllers. The band-passed CgLp still shows a less steady-state error with respect to other controllers and no large peak in control input.

VII. CONCLUSION

This article investigated the nonlinearity and higher-order harmonics for reset elements with one resetting state. A new architecture was introduced which allowed for band-passing nonlinearity in a range of frequencies and selectively reducing higher-order harmonics in a range of frequencies. After developing the HOSIDF analysis of the proposed architecture, a method called "phase shaping" was proposed for the design and tune of the introduced architecture. It was shown that FOREs such as Clegg integrator, single-state reset elements, or CgLp can be band-passed using the proposed architecture and method.

It was discussed that nonlinearity and higher-order harmonics can be beneficial in some range of frequencies such as a crossover frequency region for increasing the phase margin and can be harmful in others like lower frequencies. In the phase shaping method, the approach to eliminate nonlinearity at one frequency was also introduced which is useful for systems with a single important working frequency.

In order to validate the architecture, method, and developed theories, three controllers were designed to control a precision positioning stage. The controllers were a band-passed CgLp, a conventional one, and a PID. It was validated in practice that higher-order harmonics for band-passed CgLp at lower frequencies is much smaller than the conventional one. Moreover, it was shown that there is a clear relation between the reduction of higher harmonics at lower frequencies and the tracking precision of the system. It was verified in practice that a poorly designed conventional CgLp which performs poorly compared to PID can outperform or at least equally perform compared to PID in terms of precision in a certain range of frequencies, when the nonlinearity of conventional CgLp is

band-passed using the phase shaping method presented in the article. In other words, while the main contribution of this article was not to outperform the PID controller but to improve the performance of CgLp controllers, the current controller shows the potential to outperform the linear controllers and overcome their limitations. However, the optimal tuning of reset elements using the phase-shaping method is a subject for further studies.

Since the phase shaping method is capable of shaping the phase benefit of the reset element, one may suggest shaping the phase benefit to achieve other characteristics such as iso-damping behavior for the system or constant gain and positive phase slope. Furthermore, in this article, only the band-passed CgLp was studied in detail, investigation of band-passed Clegg, and FORE are considered future works.

REFERENCES

[1] S. P. Boyd and C. H. Barratt, *Linear Controller Design: Limits of Performance*, vol. 7. Princeton, NJ, USA: Citeseer, 1991.

[2] J. M. Maciejowski, *Multivariate Feedback Design*. Workingham, U.K.: Addison-Wesley, 1989.

[3] M. F. Heertjes *et al.*, "Control of wafer scanners: Methods and developments," in *Proc. Amer. Control Conf. (ACC)*, Jul. 2020, pp. 3686–3703.

[4] A. Baños and A. Barreiro, *Reset Control Systems*. Cham, Switzerland: Springer, 2011.

[5] Y. Guo, L. Xie, and Y. Wang, *Analysis and Design of Reset Control Systems*. London, U.K.: Institution of Engineering and Technology, 2015.

[6] J. Clegg, "A nonlinear integrator for servomechanisms," *Trans. Amer. Inst. Electr. Eng., II, Appl. Ind.*, vol. 77, no. 1, pp. 41–42, 1958.

[7] K. R. Krishnan and I. M. Horowitz, "Synthesis of a non-linear feedback system with significant plant-ignorance for prescribed system tolerances," *Int. J. Control*, vol. 19, no. 4, pp. 689–706, Apr. 1974.

[8] I. Horowitz and P. Rosenbaum, "Non-linear design for cost of feedback reduction in systems with large parameter uncertainty," *Int. J. Control*, vol. 21, no. 6, pp. 977–1001, 1975.

[9] Y. Guo, Y. Wang, and L. Xie, "Frequency-domain properties of reset systems with application in hard-disk-drive systems," *IEEE Trans. Control Syst. Technol.*, vol. 17, no. 6, pp. 1446–1453, Nov. 2009.

[10] L. Hazeleger, M. Heertjes, and H. Nijmeijer, "Second-order reset elements for stage control design," in *Proc. Amer. Control Conf. (ACC)*, Jul. 2016, pp. 2643–2648.

[11] D. Wu, G. Guo, and Y. Wang, "Reset integral-derivative control for HDD servo systems," *IEEE Trans. Control Syst. Technol.*, vol. 15, no. 1, pp. 161–167, Jan. 2007.

[12] Y. Li, G. Guo, and Y. Wang, "Nonlinear mid-frequency disturbance compensation in HDDs," in *Proc. 16th IFAC Triennial World Congr.*, Jul. 2005, pp. 151–156.

[13] Y. Li, G. Guo, and Y. Wang, "Reset control for midfrequency narrowband disturbance rejection with an application in hard disk drives," *IEEE Trans. Control Syst. Technol.*, vol. 19, no. 6, pp. 1339–1348, Nov. 2011.

[14] H. Li, C. Du, and Y. Wang, "Optimal reset control for a dual-stage actuator system in HDDs," *IEEE/ASME Trans. Mechatronics*, vol. 16, no. 3, pp. 480–488, Jun. 2011.

[15] A. Palanikumar, N. Saikumar, and S. H. HosseinNia, "No more differentiator in PID: Development of nonlinear lead for precision mechatronics," in *Proc. Eur. Control Conf. (ECC)*, Jun. 2018, pp. 991–996.

[16] C. Weise, K. Wulff, and J. Reger, "Fractional-order memory reset control for integer-order LTI systems," in *Proc. IEEE 58th Conf. Decis. Control (CDC)*, Dec. 2019, pp. 5710–5715.

[17] N. Saikumar, R. K. Sinha, and S. Hassan HosseinNia, "Resetting disturbance observers with application in compensation of bounded nonlinearities like hysteresis in piezo-actuators," *Control Eng. Pract.*, vol. 82, pp. 36–49, Jan. 2019.

[18] C. Weise, K. Wulff, and J. Reger, "Extended fractional-order memory reset control for integer-order LTI systems and experimental demonstration," *IFAC-PapersOnLine*, vol. 53, no. 2, pp. 7683–7690, 2020.

[19] D. Valério, N. Saikumar, A. A. Dastjerdi, N. Karbasizadeh, and S. H. HosseinNia, "Reset control approximates complex order transfer functions," *Nonlinear Dyn.*, vol. 97, pp. 2323–2337, Jul. 2019.

[20] M. F. Heertjes, K. G. J. Gruntjens, S. J. L. M. van Loon, N. van de Wouw, and W. P. M. H. Heemels, "Experimental evaluation of reset control for improved stage performance," *IFAC-PapersOnLine*, vol. 49, no. 13, pp. 93–98, 2016.

[21] N. Saikumar, R. K. Sinha, and S. H. HosseinNia, "'Constant in gain lead in phase' element—Application in precision motion control," *IEEE/ASME Trans. Mechatronics*, vol. 24, no. 3, pp. 1176–1185, Apr. 2019.

[22] S. J. L. M. Van Loon, K. G. J. Gruntjens, M. F. Heertjes, N. Van de Wouw, and W. P. M. H. Heemels, "Frequency-domain tools for stability analysis of reset control systems," *Automatica*, vol. 82, pp. 101–108, Aug. 2017.

[23] O. Beker, C. Hollot, Q. Chen, and Y. Chait, "Stability of a reset control system under constant inputs," in *Proc. Amer. Control Conf.*, vol. 5, Jun. 1999, pp. 3044–3045.

[24] N. Karbasizadeh, A. A. Dastjerdi, N. Saikumar, D. Valerio, and S. H. H. Nia, "Benefiting from linear behaviour of a nonlinear reset-based element at certain frequencies," in *Proc. Austral. New Zealand Control Conf. (ANZCC)*, Nov. 2020, pp. 226–231.

[25] P. W. J. M. Nuij, O. H. Bosgra, and M. Steinbuch, "Higher-order sinusoidal input describing functions for the analysis of non-linear systems with harmonic responses," *Mech. Syst. Signal Process.*, vol. 20, no. 8, pp. 1883–1904, 2006.

[26] N. Saikumar, K. Heinen, and S. H. HosseinNia, "Loop-shaping for reset control systems: A higher-order sinusoidal-input describing functions approach," *Control Eng. Pract.*, vol. 111, Jun. 2021, Art. no. 104808.

[27] A. A. Dastjerdi, A. Astolfi, N. Saikumar, N. Karbasizadeh, D. Valerio, and S. Hassan HosseinNia, "Closed-loop frequency analysis of reset control systems," 2020, *arXiv:2001.10487*.

[28] M. S. Bahnamiri, N. Karbasizadeh, A. A. Dastjerdi, N. Saikumar, and S. H. HosseinNia, "Tuning of CgLp based reset controllers: Application in precision positioning systems," *IFAC-PapersOnLine*, vol. 53, no. 2, pp. 8997–9004, 2020, doi: 10.1016/j.ifacol.2020.12.2017.

[29] A. A. Dastjerdi and S. H. Hosseinnia, "A frequency-domain tuning method for a class of reset control systems," *IEEE Access*, vol. 9, pp. 40950–40962, 2021.

[30] N. Karbasizadeh, N. Saikumar, and S. H. N. Kani, "Fractional-order single state reset element," *Nonlinear Dyn.*, vol. 104, no. 1, pp. 413–427, 2021.

[31] C. Cai, A. A. Dastjerdi, N. Saikumar, and S. H. HosseinNia, "The optimal sequence for reset controllers," in *Proc. Eur. Control Conf. (ECC)*, May 2020, pp. 1826–1833.

[32] A. Sebastian, N. Karbasizadeh, N. Saikumar, and S. H. HosseinNia, "Augmented fractional-order reset control: Application in precision mechatronics," in *Proc. IEEE/ASME Int. Conf. Adv. Intell. Mechatronics (AIM)*, Jul. 2021, pp. 231–238.

[33] R. M. Schmidt, G. Schitter, and A. Rankers, *The Design of High Performance Mechatronics-: High-Tech Functionality by Multidisciplinary System Integration*. Amsterdam, The Netherlands IOS Press, 2020.

[34] Y. Guo, L. Xie, and Y. Wang, *Analysis and Design of Reset Control Systems*. London, U.K.: Institution of Engineering and Technology, 2015.

[35] O. Beker, C. Hollot, Y. Chait, and H. Han, "Fundamental properties of reset control systems," *Automatica*, vol. 40, no. 6, pp. 905–915, 2004.

[36] A. A. Dastjerdi, N. Saikumar, and S. H. HosseinNia, "Tuning guidelines for fractional order PID controllers: Rules of thumb," *Mechatronics*, vol. 56, pp. 26–36, Dec. 2018. [Online]. Available: http://www.sciencedirect.com/science/article/pii/S0957415818301612

[37] Y. Chen, C. Hu, and K. L. Moore, "Relay feedback tuning of robust PID controllers with iso-damping property," in *Proc. 42nd IEEE Int. Conf. Decis. Control*, Dec. 2003, pp. 2180–2185.

[38] Y. Luo, Y. Chen, and Y. Pi, "Experimental study of fractional order proportional derivative controller synthesis for fractional order systems," *Mechatronics*, vol. 21, no. 1, pp. 204–214, Feb. 2011.

[39] L. Zaccarian, D. Nesic, and A. R. Teel, "First order reset elements and the CLEGG integrator revisited," in *Proc. Amer. Control Conf.*, Jun. 2005, pp. 563–568.

[40] S. H. HosseinNia, I. Tejado, and B. M. Vinagre, "Fractional-order reset control: Application to a servomotor," *Mechatronics*, vol. 23, no. 7, pp. 781–788, Oct. 2013.

[41] A. Oustaloup, "La commade CRONE: Commande robuste d'Ordre non entier," in *Hermes*. Paris, France: Hermés, 1991.

Nima Karbasizadeh (Member, IEEE) received the M.Sc. degree in mechatronics from the University of Tehran, Tehran, Iran, in 2017. He is currently pursuing the Ph.D. degree with the Department of Precision and Microsystem Engineering, TU Delft, Delft, The Netherlands.

His research during Ph.D. is focused on nonlinear control for high-precision mechatronic systems. His research interests include precision motion control, nonlinear precision control, mechatronic system design, and robotic control systems and haptics.

Ali Ahmadi Dastjerdi (Member, IEEE) received the master's degree in mechanical engineering from the Sharif University of Technology, Tehran, Iran, in 2015. He is currently pursuing the Ph.D. degree with the Department of Precision and Microsystem Engineering, TU Delft, Delft, The Netherlands.

He has also collaborated with Prof. A. Astolfi since 2019 as a sabbatical leave in Imperial College University, London, U.K. His research interests include mechatronic systems design, precision engineering, precision motion control, and nonlinear control.

Niranjan Saikumar (Member, IEEE) received the Ph.D. degree in electrical engineering with a specialization in learning controllers for mechatronic systems from the Indian Institute of Science, Bengaluru, India, in 2016.

He later worked as a Post-Doctoral Researcher with the Department of Precision and Microsystems Engineering, Mechanical Faculty, TU Delft, Delft, The Netherlands, on high-precision mechatronic systems focusing on nonlinear control and frequency domain analysis of related systems and precision mechatronic system design. Since 2021, he has been working as a System Engineer/Architect with Nearfield Instruments B.V., Rotterdam, The Netherlands, developing high-throughput AFM systems for the semiconductor industry.

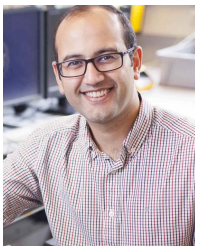

S. Hassan HosseinNia (Senior Member, IEEE) received the Ph.D. degree *(cum laude)* in electrical engineering with a specialization in automatic control: application in mechatronics in 2013.

He has an industrial background working at ABB, Västerås, Sweden. He is currently an Associate Professor with the Department of Precision and Microsystem Engineering, TU Delft, Delft, The Netherlands. He has (co)authored over 100 publications in high-impact journals, conference proceedings, and book chapters. His research interests include precision mechatronic system design, precision motion control, and mechatronic systems with distributed actuation and sensing.

Dr. HosseinNia was the General Chair of the 7th IEEE international Conference in Control, mechatronics and Automation (ICCMA 2019). He is also the Editorial Board of the following four journals: "*Fractional Calculus and Applied Analysis*," "*Frontiers in Control Engineering*," "*International Journal of Advanced Robotic Systems* (SAGE)," and "*Mathematical Problems in Engineering*."